

Electromagnetic pulses produced by a picosecond laser interacting with solid targets

Ai-Hui Niu(牛爱慧), Ning Kang(康宁), Guo-Xiao Xu(许国潇), Jia-Jie Xie(谢佳节), Jian Teng(滕建), Hui-Ya Liu(刘会亚), Ming-Ying Sun(孙明营), and Ting-Shuai Li(李廷帅)

Citation: Chin. Phys. B, 2024, 33 (**5**): 054205. DOI: 10.1088/1674-1056/ad1a95
Journal homepage: http://cpb.iphy.ac.cn; http://iopscience.iop.org/cpb

What follows is a list of articles you may be interested in

Plasmon-induced nonlinear response on gold nanoclusters

Yuhui Song(宋玉慧), Yifei Cao(曹逸飞), Sichen Huang(黄思晨), Kaichao Li(李凯超), Ruhai Du(杜如海), Lei Yan(严蕾), Zhengkun Fu(付正坤), and Zhenglong Zhang(张正龙)
Chin. Phys. B, 2024, 33 (**4**): 044204. DOI: 10.1088/1674-1056/ad1a8b

Accelerated generation of holograms with ultra-low memory symmetrically high-compressed look-up table

Yan Yang(杨燕), Jianying Zhu(朱建英), Minyuan Sun(孙敏远), and Yong Bi(毕勇)
Chin. Phys. B, 2024, 33 (**4**): 044201. DOI: 10.1088/1674-1056/ad1e67

Decoupling of temporal/spatial broadening effects in Doppler wind LiDAR by 2D spectral analysis

Zhen Liu(刘珍), Yun-Peng Zhang(张云鹏), Xiao-Peng Zhu(竹孝鹏), Ji-Qiao Liu(刘继桥), De-Cang Bi(毕德仓), and Wei-Biao Chen(陈卫标)
Chin. Phys. B, 2024, 33 (**3**): 034214. DOI: 10.1088/1674-1056/ad10fd

Gigahertz frequency hopping in an optical phase-locked loop for Raman lasers

Dekai Mao(毛德凯), Hongmian Shui(税鸿冕), Guoling Yin(殷国玲), Peng Peng(彭鹏), Chunwei Wang(王春唯), and Xiaoji Zhou(周小计)
Chin. Phys. B, 2024, 33 (**2**): 024209. DOI: 10.1088/1674-1056/ad174b

Effect of sample temperature on femtosecond laser ablation of copper

Wei-Jie Dang(党伟杰), Yu-Tong Chen(陈雨桐), An-Min Chen(陈安民), and Ming-Xing Jin(金明星)
Chin. Phys. B, 2024, 33 (**2**): 024207. DOI: 10.1088/1674-1056/ad028f

---

Electromagnetic pulses produced by a picosecond laser interacting with solid targets

Ai-Hui Niu(牛爱慧)[1,†], Ning Kang(康宁)[2,3,†,‡], Guo-Xiao Xu(许国潇)[2,4], Jia-Jie Xie(谢佳节)[1], Jian Teng(滕建)[5], Hui-Ya Liu(刘会亚)[2,3], Ming-Ying Sun(孙明营)[2,3], and Ting-Shuai Li(李廷帅)[1,§]

[1] *School of Materials and Energy, University of Electronic Science and Technology of China, Chengdu* 611731, *China*
[2] *Key Laboratory on High Power Laser and Physics, Shanghai Institute of Optics and Fine Mechanics, Chinese Academy of Sciences, Shanghai* 201800, *China*
[3] *Collaborative Innovation Center of IFSA, Shanghai Jiao Tong University, Shanghai* 200240, *China*
[4] *University of Chinese Academy of Sciences, Beijing* 100049, *China*
[5] *Science and Technology on Plasma Physics Laboratory, Research Center of Laser Fusion, China Academy of Engineering Physics, Mianyang* 621900, *China*

(Received 1 December 2023; revised manuscript received 29 December 2023; accepted manuscript online 4 January 2024)

A high-power laser ablating solid targets induces giant electromagnetic pulses (EMPs), which are intimately pertinent to laser parameters, such as energy and pulse width. In this study, we reveal the features of EMPs generated from a picosecond (ps) laser irradiating solid targets at the SG-II picosecond petawatt (PSPW) laser facility. The laser energy and pulse, as well as target material and thickness, show determinative effects on the EMPs' amplitude. More intense EMPs are detected behind targets compared to those at the other three positions, and the EMP amplitude decreases from 90.09 kV/m to 17.8 kV/m with the gold target thickness increasing from 10 μm to 20 μm, which is suppressed when the laser pulse width is enlarged. The results are expected to provide more insight into EMPs produced by ps lasers coupling with targets and lay the foundation for an effective EMP shielding design in high-power laser infrastructures.

Keywords: laser, electromagnetic pulse, target, proton

PACS: 52.40.Db, 41.75.Jv, 33.20.Xx, 42.25.Bs **DOI:** 10.1088/1674-1056/ad1a95

1. Introduction

High-power laser coupling with solid targets can generate a complex radiative environment, including hot-electrons, neutrons, protons, gamma rays, x-rays and electromagnetic pulses (EMPs),[1] among which EMPs reach hundreds of kV/m and even MV/m with a broad frequency domain extending from several MHz to GHz.[2] Intense EMPs have severely interfered with various physical diagnostics in laser–plasma experiments and even cause the malfunction of some equipment.[3] Therefore, it is essential to unveil the main factors that determine EMP amplitude and spatial evolution and, meanwhile, explore the intrinsic mechanism of EMP generation from ps lasers irradiating targets.

There are many direct or indirect laser and target parameters in relation to EMPs. Brown *et al*. from Lawrence Livermore National Laboratory adopted B-dot and D-dot probes to detect EMPs generated in the National Ignition Facility (NIF), which achieved an intensity of around 1 kV/m (laser: 19 ns, 1055 kJ) and were increased to 4 kV/m and 500 kV/m when the laser pulses were shortened to 100 ps (2 kJ) and 2 ps (132 J), indicating that EMP intensity was mostly dependent on the laser pulse.[4] Raczka *et al*. indicated that an EMP induced by laser (290 ± 20 ps, 590 ± 30 J) interaction with plastic foils reached around 620 kV/m at Prague Asterix Laser System facility.[5] Bradford *et al*. revealed the relationship between EMP energy and the total number of escaping electrons with ps laser pulse duration.[6] Our recent experimental results also confirmed that a ps pulse shooting solid targets caused more intense EMPs compared to ns and fs pulses.[7,8] Therefore, ps laser–target interaction can produce extremely intense EMPs of hundreds of kV/m, but the EMP features and the mechanisms behind them remain unexplored.

The distinct atomic density and ionization energy of materials result in a significant difference in laser energy absorption efficiency; therefore, the target materials impact EMP radiation.[9] Kugland *et al*. reported that a magnetic field caused by high-power lasers coupled to $C_2H_2Cl_2$ plastic targets with an atomic density of 6×10^{22} cm^{-3} was 2–3 times stronger than that induced by laser-coupled argon with an atomic density of 10^{20} cm^{-3}.[10] Moreover, EMPs are also related to the target configuration. Hohlraums with different configurations produce disparate EMPs, and 0.6 mg/cc of He gas filled hohlraum sharply reduced EMP intensity.[11] Since the target material and configuration were connected to escaping charged particles, Dubois *et al*. proposed a target charging model to reveal the mechanism of EMP generation.[12] The

[†]These authors contributed equally to this work.
[‡]Corresponding author. E-mail: kangning@siom.ac.cn
[§]Corresponding author. E-mail: litingshuai@uestc.edu.cn

© 2024 Chinese Physical Society and IOP Publishing Ltd

EMP amplitude was reported to be proportional to the energy of escaping hot electrons and the proton cutoff energy;[7,13] therefore, it is significant to further reveal the relationship between charged particles and EMPs induced by ps lasers.

Besides, the target material, size, thickness and configuration also affect the efficiency of target-absorbing laser energy, which in turn determine the energy and amount of emitted hot electrons, protons and charged particles associated with the characteristics of the radiated electromagnetic pulses.[14,15] Domenico *et al*. measured the target neutralization current stemming from high-power laser-coupled polyethylene targets with varying thicknesses from 0.075 mm to 1.2 mm, and the current amplitude reached the maximum value for the target thickness of 0.5 mm, which was one of the main sources of EMP generation.[16] Consoli *et al*. reported that EMP induced by a fs laser was strongly enhanced with the decrease in the plastic target thickness ranging from 550 nm to 116 nm.[17] Yilin *et al*. found that the EMP signal induced by a fs laser was lifted with the increase of the aluminum target thickness from 1.8 μm to 70 μm, and the target material also affected the EMP amplitude.[18] Therefore, there are discrepancies that exist in the effects of target thickness.

In this study, we adopt B-dot probes in four positions to detect EMPs induced by a ps laser interacting with gold and copper targets inside the PSPW laser facility. The EMP spatial distributions are analyzed and the effects of the laser energy, laser pulse and target material on EMP intensity are discussed. The correlation of EMP intensity and proton kinetic energy is revealed, and a 3D model is established to simulate EMP resonance. The results can hopefully provide a deeper understanding of the features of EMPs generated from ps laser–target interactions, and may be beneficial to the EMP shielding design for safe operation of large laser infrastructures.

2. Experimental setup

All EMP measurements were performed at the SG-II picosecond petawatt laser facility and Fig. 1(a) shows the experimental layout. A Nd:glass (∼ 1053 nm) picosecond (ps) petawatt laser beam was focused on planar film targets at the target chamber center (TCC) with an incident angle of 24°. The laser energy, pulse duration, and spot size were 50–500 J, 1–10 ps, and 10–15 μm; thus, the light intensity was about 0.4–2.5 × 10^{20} W/cm^2. The target was planar gold or copper film with a thickness of 5–20 μm, and its surfaces were along the direction of the target holder.

Several EMP probes (microstrip antennas) were placed at different angles to the target normal for the measurement of EMP signals in different directions, namely, an east probe close to the target normal and laser forward, a west probe close to the laser backward, a south probe close to the target holder, and a north probe opposite south. The antennas were installed to the holders connected to target chamber ports, as shown in Fig. 1(b); therefore, their positions were not located at the very forward or backward directions in the lack of fitted ports. The probes were connected with an oscilloscope via electromagnetic shielding cables to record EMP signals, and the signals of the four probes were comparable as the type and length of the antenna and cables of the four directions were the same.

The electric field strength (E) and energy density (ε) of EMPs are calculated as follows. Assuming the output voltage waveform recorded by the oscilloscope is $V_{\rm out}(t)$, the input voltage waveform at the probe satisfies

$$H(\omega)V_{\rm in}(\omega) = V_{\rm out}(\omega), \tag{1}$$

where $V(\omega)$ is the Fourier transform of $V(t)$, and $H(\omega)$ is the signal attenuation (response) of the probe + cables case, as shown in Fig. 1(c). Based on the conservation of power, we have

$$[E(t)^2/R_{\rm air}]A_{\rm eff} = V(t)^2/R_{\rm probe}, \tag{2}$$

where $R_{\rm air} = 377\ \Omega$ and $R_{\rm probe} = 50\ \Omega$ are the impedances of the free space and the probe, and $A_{\rm eff}$ is the effective area of the antenna. Finally, we use

$$r^2\varepsilon = \int [E(t)^2/R_{\rm air}]\,{\rm d}t \tag{3}$$

to calculate ε in units of J/sr, in which $r = 1$ m is the distance between the antennas and the EMP source (TCC).

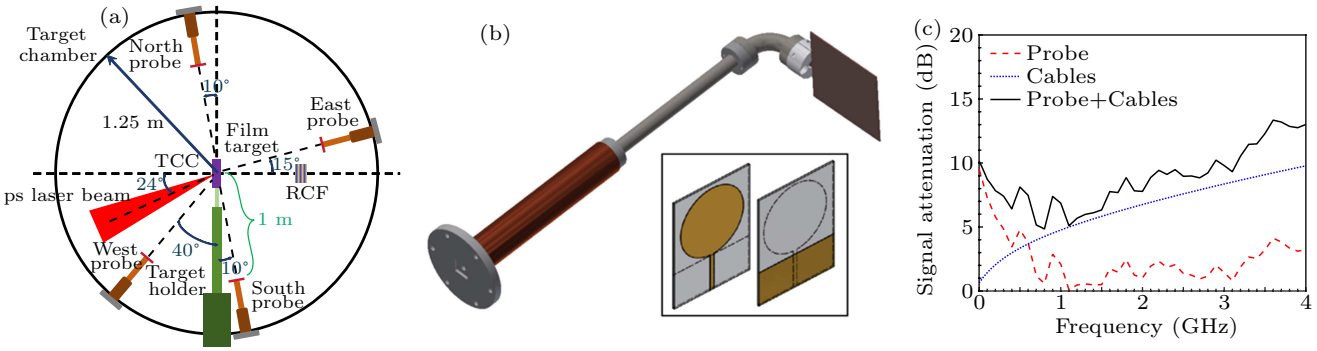


Fig. 1. (a) A schematic diagram of the experimental setup. (b) The structure of the probe and the antenna (inset). (c) Signal attenuation (response) of the probe and the cables.

Five shots were fired in the experiments: 1-ps 300-J laser on gold targets (three shots), 10-ps 500-J laser on a gold target (one shot), and 1-ps 50-J laser on a copper target (one shot). An RCF pack was placed at the back of the targets to record the maximum proton energy in the shots with the 1-ps laser and gold targets, and two of these shots had all four probes active while the west probe was not active in the other three shots.

3. Experimental results and discussion

The detailed information of the laser parameters and target parameters used in this experiment is presented in Table 1.

Figures 2(a) and 2(b) show the EMP waveform in the time domain and frequency domain. In Fig. 2(a), EMP signals last for around 100 ns before decaying to noise, and the maximum strength (E_{max}) reaches about 100 kV/m. The variation of E_{max} can be attributed to the target material, target thickness and laser pulse duration. In Fig. 2(b), signals are mainly found within the frequency range of 0.1–2 GHz, which is consistent with previous reports under similar conditions.[2] Typical peaks at 0.27 GHz, 0.45 GHz, 0.65 GHz and 1 GHz are observed in these shots, which can be attributed to the emission of hot electrons and the formation of a discharge current.

Table 1. Laser parameters and target parameters for each shot in this experiment.

No.	Laser pulse (ps)	Laser energy (J)	Target thickness (μm)	Target material	Probe position
1	1	358	5	gold	north
2	1	358	5	gold	east
3	1	358	5	gold	south
4	1	328	10	gold	north
5	1	328	10	gold	east
6	1	328	10	gold	south
7	1	328	10	gold	west
8	1	334	20	gold	north
9	1	334	20	gold	east
10	1	334	20	gold	south
11	1	334	20	gold	west
12	10	501	10	gold	north
13	10	501	10	gold	east
14	10	501	10	gold	south
15	1	56	20	copper	north
16	1	56	20	copper	east
17	1	56	20	copper	south

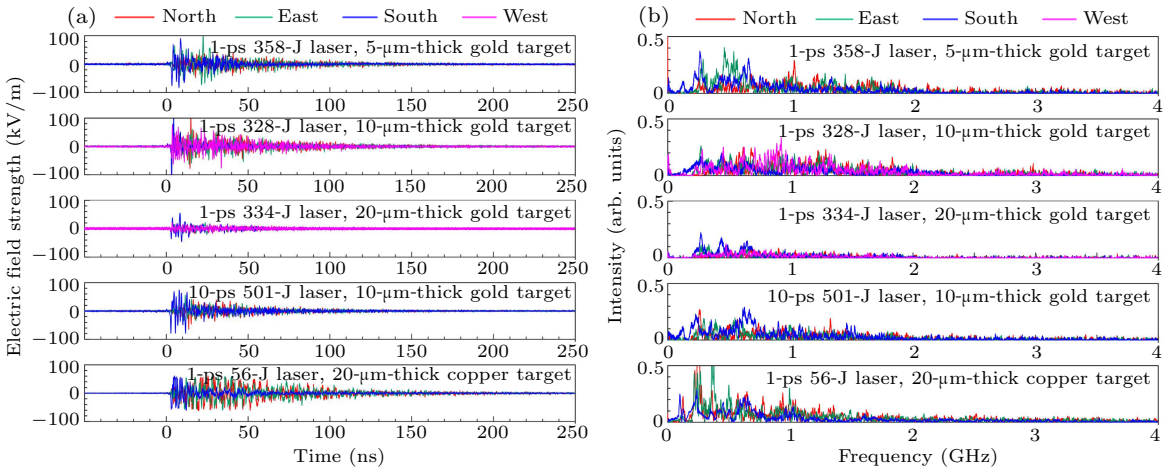


Fig. 2. (a) Waveforms of EMPs in the time domain and (b) the frequency domain. The EMPs detected by north/east/south/west probes correspond to the lines with colors of red/green/blue/purple. Note that the west probe is active only in the shots shown in rows 2 and 3.

Figure 3(a) shows the evolution of the maximum electric field with laser energy, where the effect of laser energy is less determinative compared to the detected positions, indicating that EMPs are obviously polarized. EMPs measured by the south probe surpass those in other directions, especially when the laser energy is higher than 300 J, which is mainly because more hot electrons are generated behind the target, in good agreement with previous reports.[7,19] Besides, the south probe is mostly close to the target stalk, which mainly collects EMPs induced by the neutralization current.[1] The other EMP signals have similar E_{max} and ε in many shots, indicating that EMP distributions in the target chamber are roughly

spherically symmetric, differing from the strong directionality of ionizing radiation. As the EMP signal lasts for hundreds of nanoseconds, its distribution can be reshaped by the cavity through iterative reflections; therefore, the symmetrical distribution is attributed to chamber resonance. As shown in Fig. 3(b), the conversion efficiency from laser to EMP (based on the spherically symmetrical distribution) is about 1% for the copper targets and 1‰ for the gold targets. Moreover, the comparison between the 10-ps 500-J and 1-ps 300-J laser coupling with 10-μm-thick gold targets suggests that the EMP strength is mainly determined by laser intensity instead of energy, which is supported by previous conclusions.[16]

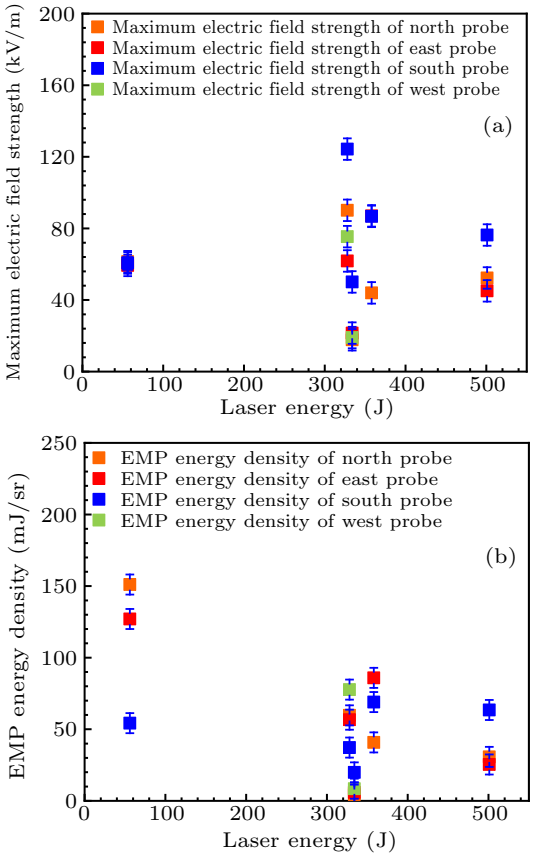


Fig. 3. (a) The maximum electric field (E_{max}) and (b) EMP energy density (ε) versus laser energy corresponding to Fig. 2.

Figure 4 shows the relation between E_{max} (ε) and the maximum proton kinetic energy ($KE_{p,max}$) under the conditions of a 1-ps laser interacting with gold targets, where $KE_{p,max}$ is positively correlated with E_{max} and ε, and it shows a linear relation between $KE_{p,max}$, and E_{max}. The emission of protons should be pulled out by escaping hot electrons; therefore, the higher $KE_{p,max}$ accounts for stronger EMP radiation, which has been proved by our previous report.[20] Figure 5 shows the spatial distribution of EMPs detected at four different positions within the target chamber. The laser parameters and target parameters are also presented in Fig. 5. EMPs detected by the south probe and east probe are generally more intense than those measured by the other two probes, which possibly results from the larger number of hot electrons emitting behind the target and the neutralization current.[8,16]

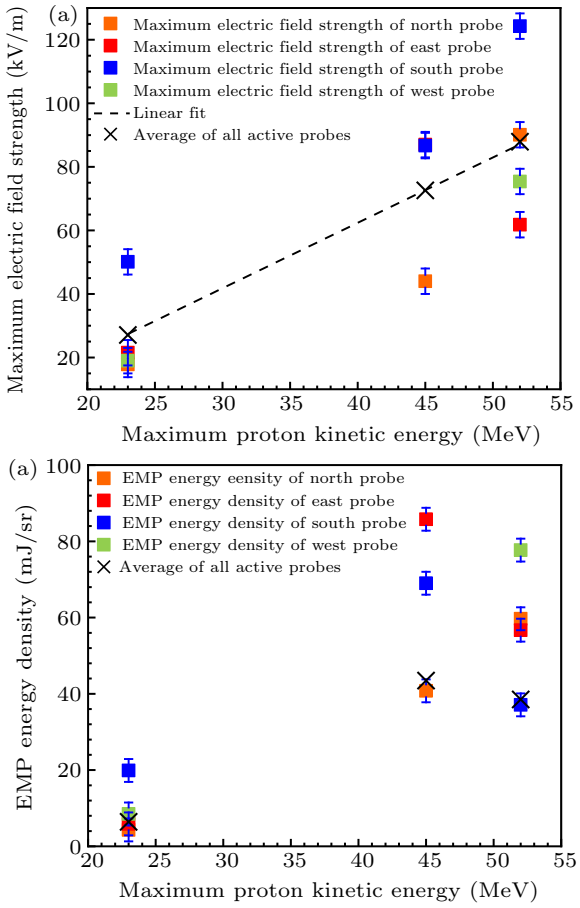


Fig. 4. (a) Evolution of E_{max} and (b) ε with the maximum proton kinetic energy detected from a 1-ps laser interacting with gold targets. The crosses represent the average values of all active probes, and the black dashed line represents the linear fitting for the crosses.

Figure 6 shows the effects of laser energy, target material and thickness on EMP intensity. Adjusting the pulse from 10 ps to 1 ps is more effective at enhancing the EMP than lifting the energy, as shown in Fig. 6(a), and Fig. 6(b) shows that the copper target is more advantageous to achieve a larger EMP amplitude over the gold target. Since the resistivity of copper (1.7×10^{-8} Ω·m) is lower than that of gold (2.4×10^{-8} Ω·m), according to Ohm's law

$$E = \eta J_e, \tag{4}$$

where η is the resistivity of the bulk target, and J_e is the current density of electrons. An intense resistive electric field inhibits the transport of hot electrons, suggesting the enhanced resistive electric fields can cause a significant decrease in the number as well as the energy of hot electrons during ejection.[21] A larger electrical conductivity results in lower resistance to electron transport within the target and lower energy loss, which possibly leads to both a greater number and energy of hot electrons exiting behind the target.[22] Thus, the laser pulse and target material are more advantageous over laser energy with regard to the enhancement of EMP intensity.

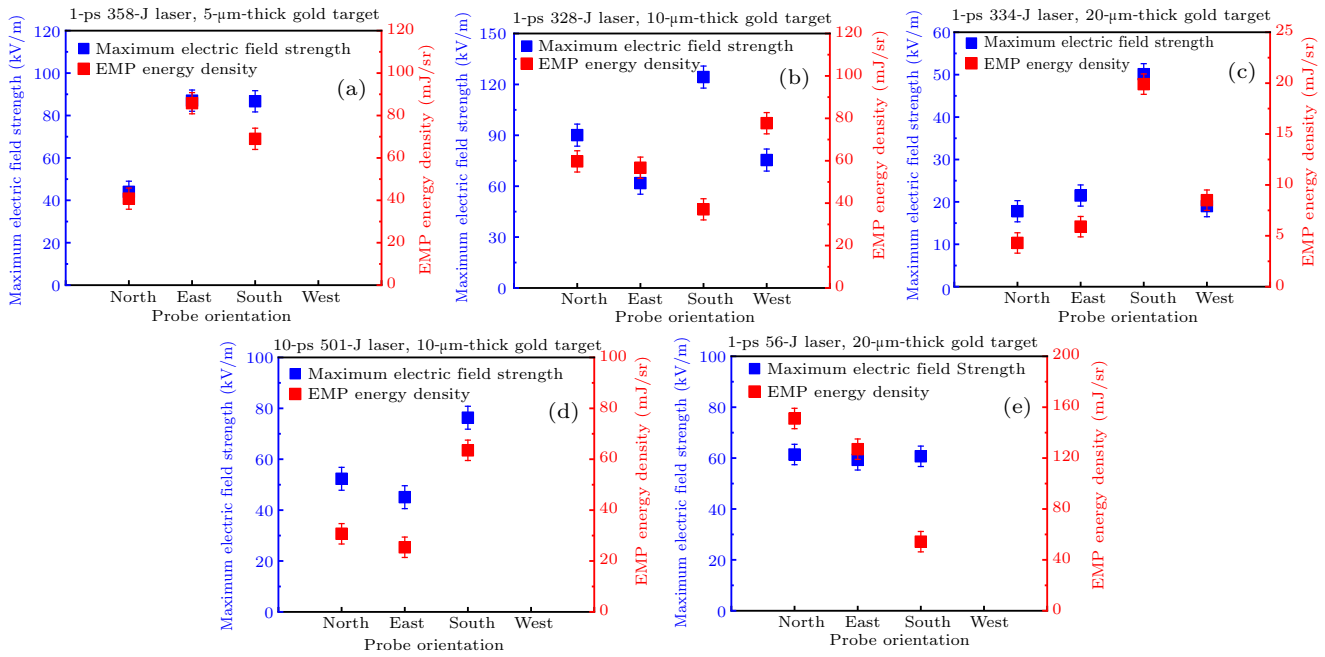


Fig. 5. EMP intensity at four positions induced by (a) a 1-ps, 358-J laser coupled with a 5-μm thick gold target; (b) a 1-ps, 328-J laser with a 10-μm thick gold target; (c) a 1-ps, 334-J laser with a 20-μm thick gold target; (d) a 10-ps, 50-J laser with a 10-μm thick gold target; (e) a 1-ps, 56-J laser with a 20-μm thick gold target.

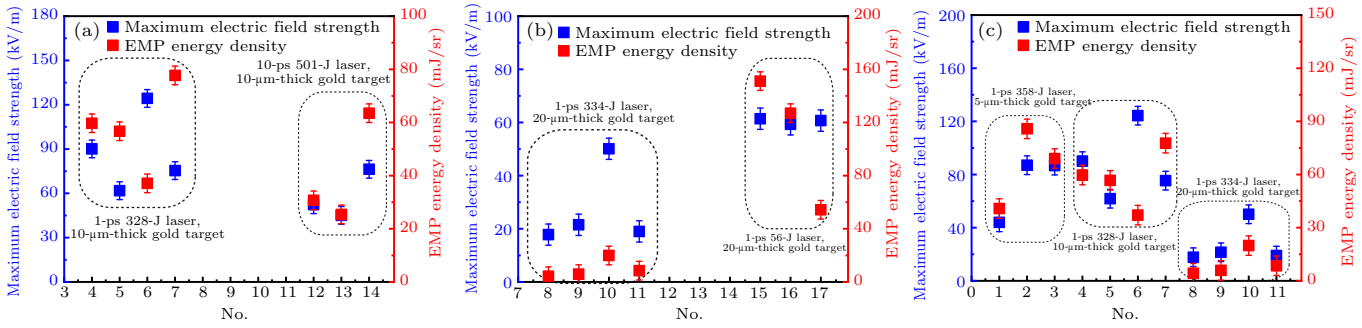


Fig. 6. The evolution of the maximum electric field strength: (a) effect of the laser pulse, (b) effect of the target material, and (c) effect of target thickness. See detailed information in Table 1.

At the SG-II picosecond petawatt (PSPW) laser facility, when the gold target thickness is increased from 5 μm to 10 μm, the maximum electric field is slightly strengthened, but it is obviously reduced if the gold target thickness is continuously increased to 20 μm, as displayed in Fig. 6(c). Although EMP intensity is positively correlated with laser energy,[21] the pulse can affect the EMP to the largest extent, even compared to the target material.[7,8] With the laser duration increasing, the energy and number of escaping electrons are reduced, which lead to a decrease in the EMP intensity.[6,22,23] Meanwhile, when the target thickness is increased from 10 μm to 20 μm, the laser incident into the target causes a reduction in the number and energy of emitted protons.[22,24]

The uncompensated positive charge at the target surface by the escaped electrons creates the background potential $\varphi_{\rm bg}$, which can be estimated by

$$\varphi_{\rm bg} = Q/(2\pi\varepsilon d), \tag{5}$$

where ε is the relative dielectric constant.[21] As the proton energy stems partly from the kinetic energy obtained after acceleration of the electric field and the corresponding field strength is strongly dependent on the polarized charge stored in the residual target, the larger proton energy leads to more intense polarization strength.[25,26] Therefore, adjustment of target thickness is useful for controlling the EMP intensity.

Based on the results in Fig. 2, we find that EMPs mostly distribute in frequency domains ranging from 0.1 GHz to 2 GHz. As shown in Fig. 7(a), to reveal the contribution from resonance to the frequency spectra, a simplified ideal 3D model is constructed to simulate the resonant frequency. The model is built as a spherical target chamber with an inner radius of 1250 mm and a thickness of 50 mm, and target holders (Φ is the diameter and L is the length) are set as cylindrical in multiple sections from the interior of the target chamber pointing to the target in the following order $(\Phi,\ L) = (340,\ 225)$, (240, 290), (50, 590), (10, 95) and (3, 50), in which the units are all in mm. The probe bracket is a discus-like shape with a thickness of 20 mm and a radius of 1080 mm, and its upper surface is located in the center of the target chamber. The simulated results are presented in Fig. 7. Note that this simulation

is simplified inside the target chamber without including some real equipment in the model.

The simulated frequency peaks of EMPs firstly depend on the eigenmodes excited within the laser chamber as a resonator. As shown in Fig. 7(c), modes 1 and 2 refer to an empty target chamber with the smallest oscillation frequency of around 0.1 GHz. Modes 3 to 8 refer to an ideal model of the target chamber, including a target holder and a probe bracket. In reality, there is other equipment inside the target chamber; therefore, some additional instruments are included in modes 9 and 10. The resonant frequency of the empty target chamber is simulated to 0.1 GHz, and the resonant frequencies of the ideal model of the target chamber are simulated from 0.11 GHz to 0.14 GHz. The simulated frequency of the target chamber with equipment reaches 0.19 GHz, lower than the characteristic frequency, as shown in Fig. 2(b), which can be attributed to various possible sources of EMPs and the effects of some internal real arrangements in the target chamber.[8,18] The obtained frequencies are similar to some reported results. At the XG-III laser facility, resonant frequencies (TE111, TM010, TE011) were calculated by simplifying the chamber based on the ideal cylindrical target chamber models, where three typical resonant frequencies of 140.4 MHz, 104.9 MHz and 210 MHz were obtained.[7] For the Vulcan petawatt laser at the Rutherford Appleton Laboratory (RAL), the resonant modes of the chamber were calculated to 76 MHz, 82 MHz and 101 MHz.[2] Yang *et al.* established a model to simulate the target chamber resonance, which reached 24.80 MHz, 25.06 MHz, 31.72 MHz, 43.58 MHz, 48.13 MHz, 61.48 MHz, 61.52 MHz, 64.01 MHz and 68.01 MHz.[8]

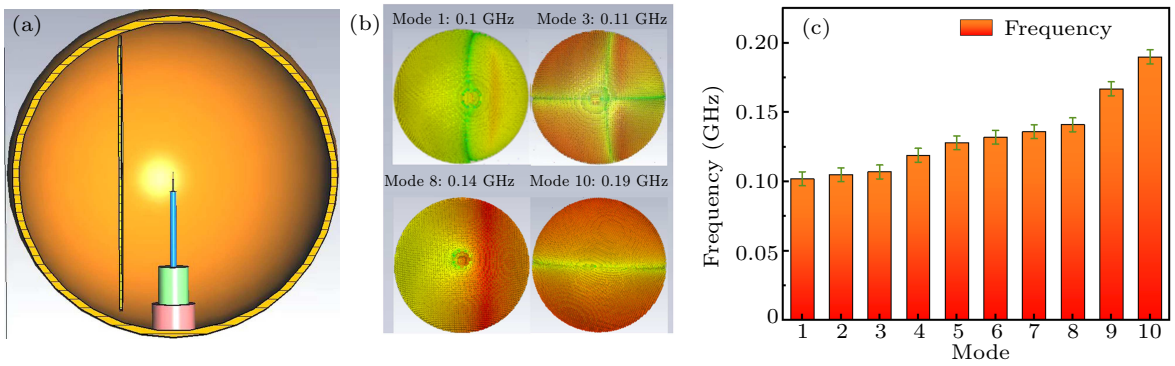


Fig. 7. The simulation layout, including the target chamber, the probe bracket and target stalk, in the model. (a) A cross-section of the model. (b) The model scheme and normalized electric field distributions corresponding to the resonant frequencies of 0.1 GHz, 0.11 GHz, 0.14 GHz and 0.19 GHz. (c) Simulated resonance frequencies for different modes.

4. Conclusion

EMPs are generated from a ps laser irradiating solid targets at the PSPW laser facility. EMPs are strongly related to laser pulse width, and decrease as the laser pulse width increases. The target thickness and material determine the number and energy of the escaping hot electrons and thus determine EMPs, which are proportional to the maximum proton kinetic energy, suggesting that the charged ion is one of the main original sources of EMPs. The resulting conclusions are expected to provide a deep understanding of EMPs induced by ps laser–target interaction and lay the foundation for EMP shielding designs.

Data availability statement

The data that support the findings of this study are available from the corresponding authors upon reasonable request.

Acknowledgements

Project supported by the Strategic Priority Research Program of the Chinese Academy of Sciences (Grant No. XDA25020205) and the program of Science and Technology on Plasma Physics Laboratory, China Academy of Engineering Physics (Grant No. 6142A04220108).

References

[1] Marco M D, Krása J, Cikhardt J, Velyhan A, Pfeifer M, Dudžák R, Dostál J, Krouský E, Limpouch J, Pisarczyk T, Kalinowska Z, Chodukowski T, Ullschmied J, Giuffrida L, Chatain D, Perin J P and Margarone D 2017 *Phys. Plasmas* **24** 083103

[2] Consoli F, Tikhonchuk V T, Bardon M, Bradford P, Carroll D C, Cikhardt J, Cipriani M, Clarke R J, Cowan T E, Danson C N, Angelis R D, Marco M D, Dubois J L, Etchessahar B, Garcia A L, Hillier D L, Honsa A, Jiang W M, Kmetik V, Krasa J, Li Y T, Lubrano F, McKenna P, Metzkes-Ng J, Poye A, Prencipe I, Raczka P, Smith R A, Vrana R, Woolsey N C, Zemaityte E, Zhang Y H, Zhang Z, Zielbauer B and Neely D 2020 *High Power Laser Sci.* **8** e22

[3] Xia Y D, Zhang F, Cai H B, Zhou W M, Tian C, Zhang B, Liu D X, Yi T, Xu Y L, Wang F, Li T S and Zhu S P 2020 *Matter Radiat. Extremes* **5** 017401

[4] Brown C G, Clancy T J, Eder D C, Ferguson W and Throop A L 2013 *The European physical Journal Conferences* **59** 08012

[5] Rączka P, Cikhardt J, Pfeifer M, Krasa J, Krupka M, Burian T, Krůs M, Pisarczyk T, Dostal J and Dudžák R and Badziak J 2021 *Plasma Phys. Contr. F.* **63** 085015

[6] Bradford P, Woolsey N C, Scott G G, Liao G, Liu H, Zhang Y, Zhu B, Armstrong C, Astbury S, Brenner C, Brummitt P, Consoli F, East I, Gray R, Haddock D, Huggard P, Jones P J R, Montgomery E, Musgrave I, Oliveira P, Rusby D R, Spindloe C, Summers B, Zemaityte E, Zhang Z, Li Y, McKenna P and Neely D 2018 *High Power Laser Sci.* **6** e21

[7] He Q Y, Deng Z G, Meng L B, Zhang Z M, Cui B, Qi W, Yang L, Liu H J, Fan W, Wang C K, Yi T, Gu Y, Lin C, Consoli F, Zhou W M and Li T S 2022 *Nucl. Fusion* **62** 066006

[8] He Q Y, Kang N, Ren L, Tian C, Wang C K, Zhang Z M, Liu D X, Yang L, Liu H Y, Sun M Y, Zhu B Q, Zhou W M and Li T S 2021 *Plasma Sci. Technol* **23** 115202

[9] Duchateau G, Yamada A and Yabana K 2022 *Phys. Rev B* **105** 165128

[10] Kugland N L, Aurand B, Brown C G, Constantin C G, Everson E T, Glenzer S H, Schaeffer D B, Tauschwitz A and Niemann C 2012 *Appl. Phys. Lett.* **101** 024102

[11] Yang Y, Guo X D, Li Z H, He Q Y, Xiong G, Li H, Yu B, Wang C K, Yang J M, Yi T, Wang F and Li T S 2022 *IEEE T. Nucl. Sci.* **69** 2027

[12] Dubois J L, Lubrano-Lavaderci F, Raffestin D, Ribolzi J, Gazave J, Fontaine A C L, D'Humières E, Hulin S, Nicolaï P, Poyé A and Tikhonchuk V T 2014 *Phys. Rev E* **89** 013102

[13] Xia Y D, Zhang F, Cai H B, Zhou W M, Tian C, Zhang B, Liu D X, Yi T, Xu Y L, Wang F, Li T S and Zhu S P 2017 *Matter Radiat. Extrem.* **5** 017401

[14] Minenna D F G, Poyé A, Bradford P, Woolsey N and Tikhonchuk V T 2020 *Phys. Plasmas* **27** 063102

[15] Qi R, Zhou C L, Zhang D D, Song L W, Yang X J, Gui J Y, Leng Y X, Tian Y and Li R X 2022 *Appl. Sci* **12** 6059

[16] Side D D, Caricato A P, Krása J and Nassisi V 2018 *Appl. Phys. A-Mater* **124** 138

[17] Consoli F, Angelis R D, Robinson T S, Glitrap S, Hicks G S, Ditter E J, Ettlinger O C, Najmudin Z, Notley M and Smith R A 2019 *Sci. Rep.* **9** 8551

[18] Xu Y L, Li D Y, Xia Y D, Zhang S Y, Wu M J, Yang T, Zhu J G, Cheng H, Wang C K, Lin C, Li T S and Yang X Q 2022 *Chin. Phys. B* **31** 025205

[19] Yang Y M, Yi T, Yang M, Wang C K and Li T S 2018 *Laser Phys.* **29** 016003

[20] Liao Q, Wu M J, Gong Z, Geng Y X, Xu X H, Li D Y, Shou Y R, Zhu J G, Li C C, Yang M, Li T S, Lu H Y, Ma W J, Zhao Y Y, Lin C and Yan X Q 2018 *Phys. Plasmas* **25** 063109

[21] Poyé A, Hulin S, Bailly-Grandvaux M, Dubois J L, Ribolzi J, Raffestin D, Bardon M, Lubrano-Lavaderci F, D'Humières E, Santos J J, Nicolaï P and Tikhonchuk V 2015 *Phys. Rev E* **91** 043106

[22] Geng Y X, Wu D, Yu W, Sheng Z M, Fritzsche S, Liao Q, Wu M J, Xu X H, Li D Y, Ma W J, Lu H Y, Zhao Y Y, He X T, Chen J E, Lin C and Yan X Q 2020 *Matter Radiat. Extrem* **5** 064402

[23] Li S P, Wang X C, Chen G J and Wang Z K 2023 *Micromachines-Basel* **14** 119

[24] Kuri D, Nilakshi D and Kartik P 2017 *Appl. Phys. B* **123** 201

[25] Delion D S and Dumitrescu A 2021 *Phys. Rev. C* **103** 054325

[26] Budaca R and Budac A I 2017 *Eur. Phys. J. A* **53** 160